UNIVERSITA' DEGLI STUDI DI PADOVA

DIPARTIMENTO DI INGEGNERIA DELL'INFORMAZIONE

Corso di Laurea Magistrale in Bioingegneria

Segmentation of the retinal vasculature of the infant eye fundus: a comparison among vesselness measures

Relatore: Prof. Alfredo Ruggeri
Correlatore: Ing. Enea Poletti

Laureando: Alberto Gozzo

Anno Accademico 2012 - 2013

Ai miei genitori

Abstract

Retinopathy of Prematurity (ROP) is a serious eye disease that affects premature infants. The earliest signs of ROP are increased tortuosity and dilation of retinal vessels. Nowadays, clinicians base their diagnosis only on subjective visual inspection. Automatic segmentation of the vasculature in retinal images is important in the detection of this type of disease because it can aid physicians during their diagnosis. This thesis describes different *vesselness measures* for the retinal fundus of the infant eye and presents a comparison among vessel detection's approaches. We consider three different detection methods, i.e., *Line Strength, Matched Filter* and *Eigen-decomposition of the Hessian*. Then, for the best values of accuracy provided by the previous methods, an algorithm based on the direction coherency measure is proposed to enhance performances. In the future, our algorithm can be further improved to provide even better results in terms of accuracy.

Sommario

La Retinopatia del Prematuro (ROP) è una malattia grave che colpisce i bambini nati prematuri. I primi segnali del manifestarsi della malattia sono un'eccessiva tortuosità e dilatazione dei vasi della retina. Al giorno d'oggi, i clinici basano la propria diagnosi sull'esperienza diretta che hanno sulla malattia attraverso l'analisi visiva. La segmentazione automatica della vascolarizzazione in immagini retiniche può essere un valido aiuto per supportare le decisioni del personale sanitario durante la diagnosi e le relative cure. Questa tesi descrive le varie misure di vesselness per immagini di neonato e mostra un confronto fra differenti approcci alla corretta segmentazione. Come algoritmi di vessel tracking si sono utilizzati *Line Strength, Matched Filter* e *Eigen-decomposition of the Hessian*. Di queste misure, si tengono conto in seguito dei migliori risultati in termini di accuratezza. Viene poi proposta una misura di coerenza legata alla direzionalità di ciascun pixel dell'immagine per migliorare le prestazioni dei precedenti metodi. In futuro, questo nuovo algoritmo può essere migliorato e fornire risultati più performanti.

Contents

1 Introduction **1**
- 1.1 Retinopathy of Prematurity . . . 2
  - 1.1.1 Short history . . . 2
  - 1.1.2 Pathogenesis: two phases of ROP . . . 2
  - 1.1.3 Screening for ROP disease . . . 3
  - 1.1.4 Treatment . . . 4
- 1.2 Outline of this thesis . . . 5

2 Theoretical overview **7**
- 2.1 Line Strength . . . 7
- 2.2 Eigen-decomposition of the Hessian . . . 8
- 2.3 Matched Filter . . . 10

3 Vessel segmentation **13**
- 3.1 Receiver Operating Characteristic . . . 13
- 3.2 Line Strength . . . 15
- 3.3 Eigen-decomposition of the Hessian . . . 17
- 3.4 Matched Filter . . . 18

4 Direction coherency measure **23**
- 4.1 Line Strength . . . 23
- 4.2 Eigen-decomposition of the Hessian . . . 26
- 4.3 Matched Filter . . . 27

5 Conclusion **31**

Bibliography **33**

List of figures **36**

List of tables **37**

Chapter 1

Introduction

Retinal vessel segmentation is important in the detection of numerous eye diseases and plays an important role in the automatic retinal disease screening system. Some diseases, e.g., retinopathy of prematurity (ROP), affect the morphology of the vessel tree itself. In fact, ROP is categorised by the zone, stage and presence of "plus disease". In plus disease, abnormal blood flow in the retina results in the dilation and tortuosity of the major retinal arteries and veins in the posterior pole. Plus disease is a sign that ROP is worsening, and may require treatment.

Regional shortages in the availability of ophthalmologists able to provide ROP diagnostic examinations are a substantial barrier to ensuring appropriate worldwide ROP care. Automatic segmentation of the vasculature in retinal images is important in the detection of this type of disease because it can aid physicians during their detections.

Nowadays, clinicians base their opinions only on their direct experience of the disease. To overcome the inherent inaccuracies in qualitative evaluation, a computer can automatically detect the disease or, at least, it can provide guidelines useful for diagnosis. Several groups have explored the use of the automatic techniques [1]-[4] to analyse ROP disease but until now none of them has advanced to the stage of being widely used as a clinical tool.

This thesis describes vesselness measures for the retinal fundus of the infant eye and proposes a comparison of different approaches. This introductory chapter provides some background information on ROP disease such as its phatogenesis, screening and treatment, and concludes with an outline of the thesis.

1.1 Retinopathy of Prematurity

Retinopathy of Prematurity (ROP) [5] is a serious eye disease that affects premature infants. It can be mild and resolve spontaneously, but in more serious cases it becomes very aggressive: new blood vessel formation progresses to scarring, retinal detachment and blindness. Figure 1.1 shows the anatomy of the human eye with the most important features labelled.

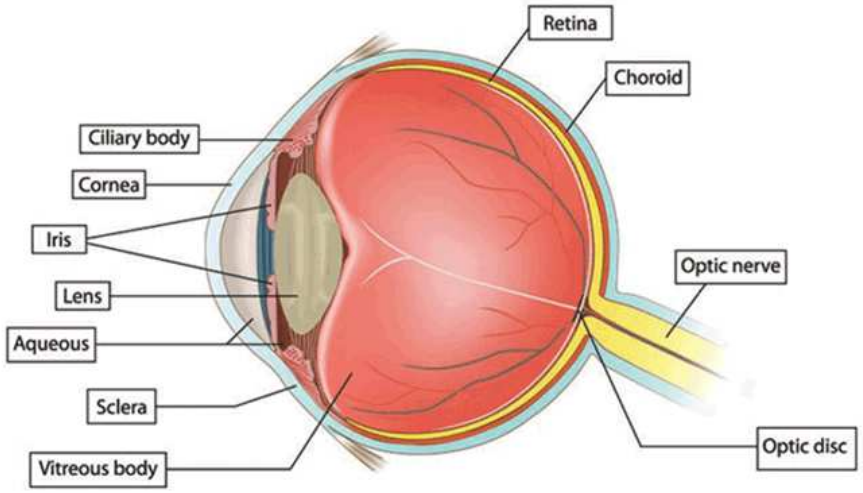

Figure 1.1: Cross sectional view of the human eye.

1.1.1 Short history

Formerly known as retrolental fibroplasia, ROP was originally described in the 1940s by Terry who first connected the condition with premature birth [6]. At that time, no treatment for ROP was available. Major advances in ROP treatment came in the 1980s and 1990s, when cryotherapy and laser photocoagulation of the avascular retina were shown to be partially effective in preventing blindness in ROP infants. Despite these ablation treatments reducing the incidence of blindness by 25% in infants with late-stage disease, patients still often have poor visual acuity after treatment. Preventive and less destructive therapies for ROP would be much more desirable, and understanding the molecular basis of the disease is important in the development of such medical interventions.

1.1.2 Pathogenesis: two phases of ROP

ROP is a biphasic disease consisting of an initial phase of vessel loss followed by a second phase of vessel proliferation. For a better understanding of the process, one needs to examine the development of retinal vasculature. Retinal vascularisation originates

from the centre of the optic disc and progresses radially outwards towards the ora serratta. Retinal blood vessel development in humans is initiated during the fourth month of gestation and reaches the retinal periphery just before birth [7]. Therefore, infants born prematurely have incompletely vascularised retinas with a peripheral avascular zone. The gestational age at birth of the premature infant determines the area of the avascular zone.

In premature infants, vascular growth that would normally occur in utero slows or ceases and is accompanied by regression of developed retinal vessels. As the infant matures, the non-vascularised retina becomes increasingly metabolically active and, in the absence of an adequate vascular system, leads to tissue hypoxia. The first phase of ROP occurs from birth to approximately 30-32 weeks postmenstrual age.

The second phase of ROP is characterised by hypoxia-induced retinal neovascularisation and begins at around 32-34 weeks postmenstrual age. This phase of ROP is similar to the neovascularisations in other proliferative retinopathies such as diabetic retinopathy. New vessels form at the junction between the vascularised retina and the avascular zone of the retina. Over time, this pathological growth of vessels produces a fibrous scar extending from the retina to the vitreous gel and lens. Retraction of this scar tissue can separate the retina from the retinal pigment epithelium, resulting in retinal detachment and likely blindness.

1.1.3 Screening for ROP disease

RetCam [8] is a wide angle pediatric retinal imaging system useful for screening ROP. It is a non stressful way to screen premature babies and is easier to perform compared to indirect ophthalmosocopy done by ophthalmologists.

The RetCam can directly image the angle, and they share hardware consisting of a handheld digital video camera connected fibre-optically to a light-emitting control unit and computer assembly. The operator controls focus, illumination, and acquisition of images with a foot switch. A short video stream is captured with still frames saved from the video at the end of the imaging session. The video mode helps to overcome movement on the part of the patient or operator and thus allows for the acquisition of clear, well-focused frames.

For the anterior segment, the operator uses the same lens as for imaging infants. In our case the 130° fundus lens (also known as the ROP lens) attached to the camera are used. Instead of sitting at the slit lamp, subjects are in a semisupine position on a bed or reclining chair, while the operator approaches them from behind the top of their heads. To maintain a reproducible point of reference, the operator should keep the cable connecting the camera to the RetCam's mainframe in a 12 o'clock orientation to the patient.

The main drawbacks of RetCam images, with respect to images provided by the standard fundus cameras used for the adult patients, are:

- presence of interlacing artifacts, as images are actually single frames extracted

from video;

- narrow blood vessels, due to the wide-field of view coupled with the 640×480 pixel resolution;
- non uniform illumination in the captured wide field of view;
- high visibility of choroidal vessels, related to the lack of pigmentation of the infant choroid.

All these aspects make the automatic analysis of RetCam images quite challenging and custom techniques are therefore necessary to successfully trace the vasculature. In Figure 1.2 there are two examples of wide-field ROP image.

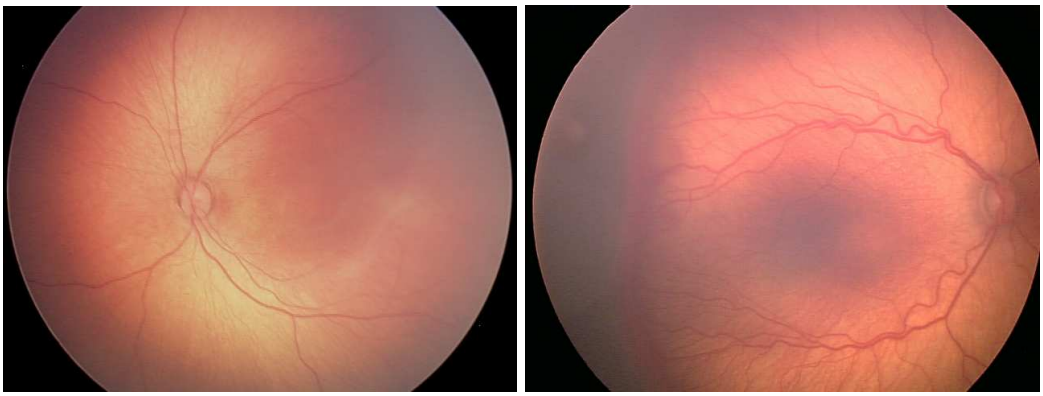

Healthy Pathological (ROP disease)

Figure 1.2: Two examples of wide-field ROP image.

1.1.4 Treatment

Early treatment has been shown to improve a baby's chances for normal vision. Treatment should start within 72 hours of the eye exam.

Some babies with "plus disease" need immediate treatment. Treatment may include cryotherapy (freezing) to prevent the spread of abnormal blood vessels.

Laser therapy (photocoagulation) may be used to prevent complications of advanced ROP. Laser therapy stops the abnormal blood vessels from growing and can be performed in the nursery using portable equipment. To be effective, it must be done before scarring and detachment occur.

Surgery is needed if the retina detaches. Surgical procedures continue to improve, but may not result in good vision.

1.2 Outline of this thesis

This thesis describes different approaches for vessel enhancement or mathematically defined "vesselness measures".

Chapter 2 provides a theoretical overview of several different techniques for the automatic detection of the vasculature in retinal images. These techniques are used in all subsequent chapters. We considered the vesselness measure based on the *Line Strength, Matched Filter* and *Eigen-decomposition of the Hessian*.

In chapter 3 a comparative analysis is performed using ROC curves. For each method, described in Chapter 2, the ROC curves at different lengths or scales are shown and the results are discussed.

In chapter 4 a new algorithm is proposed with the aim of improving vesselness performances. The direction coherency measure uses the "direction map" that provides an angular value for all the pixels in the image. This new algorithm uses a measure of direction to find vessels that have a strong probability of being correctly classified. The ROC curves are performed to show results and make comparisons.

Finally, Chapter 5 provides a brief conclusion.

Chapter 2

Theoretical overview

This chapter provides an overview of different approaches in vessel segmentation, i.e., *Line Strength, Matched Filter* and *Eigen-decomposition of the Hessian*. A theoretical approach is provided in order to present the state of the art in this field.

2.1 Line Strength

This study is based on the evaluation of pixel lines at multiple orientations.

At the beginning, it is useful to work on the inverted green channel images, where vessels appear brighter than the background. To preserve the image in the sense of vessel structure, preprocessing on the image is not made.

The average grey level is evaluated along lines of fixed length l passing through the target pixel (i, j) at different orientations. Ricci and Perfetti [9] evaluate 12 angles each of 15 angular resolution as the best choice on adult images. We use this setup for our ROP images.

The line with the largest average grey level is considered. This value is denoted with $L(i, j)$. The difference $S(i, j) = L(i, j) - N(i, j)$ represents the *line strength* of the pixel [14], where $N(i, j)$ is the average grey level in the square window, centered on the pixel, with edge length equal to l.

The basic line detector is illustrated in figure 2.1 and 2.2 (a).

The line strength is large if the winning line is aligned within a vessel. Otherwise, we have a partial overlap and the line strength is lower. This difference allows the operator to discriminate vessel pixels from non-vessel pixels. Lines of different lengths have been considered as a working parameter for the simulation setup.

The square window is not oriented like the winning line but is kept fixed. Moreover, the average grey level of lines is not obtained by interpolation. In fact, the pixels to be averaged are found by rounding the coordinates of the points on the ideal line.

The basic line detector described above can be improved for retinal vessel segmentation. In proximity of a large and bright vessel, the line strength of a pixel can be

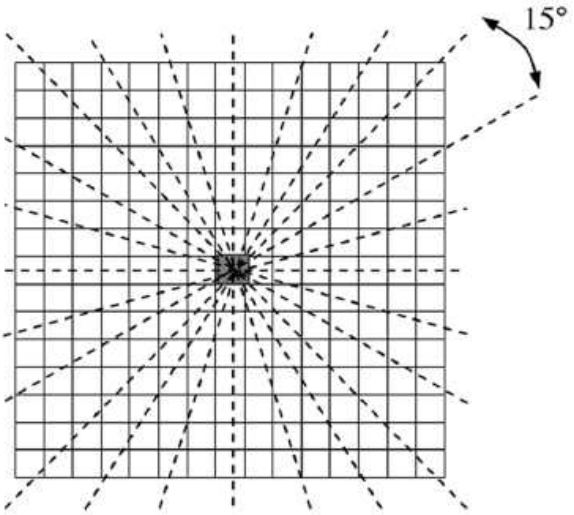

Figure 2.1: Twelve orientations to evaluate line strength of shaded pixel.

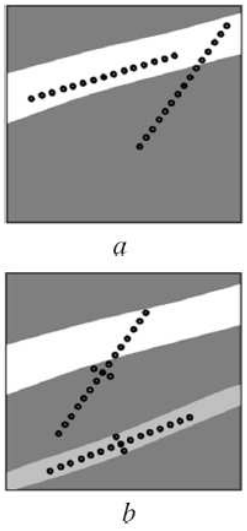

Figure 2.2: (a) Basic line detector. (b) Line detector with its orthogonal line.

comparable with that of the pixel inside a darker and thinner vessel. A possible way to overcome this problem [9] is an orthogonal line, centred on the midpoint of the main line, has length of three pixel [Figure 2.2 (b)]. This additional information helps to discriminate between inside and outside pixels

For simplicity, we consider only the line strength approach in its basic form.

2.2 Eigen-decomposition of the Hessian

In [12] vessel enhancement is designed as a filtering process that searches for geometrical structures which can be regarded as tubular.

A common approach to analyse the local behaviour of an image, L, is to consider its Taylor expansion in the neighbourhood of a point x_o,

$$L(x_o + \delta x_o, s) \approx L(x_o, s) + \delta x_o^T \nabla_{o,s} + \delta x_o^T H_{o,s} \delta x_o. \tag{2.1}$$

This expansion approximates the structure of the image up to second order. $\nabla_{o,s}$ and $H_{o,s}$ are the gradient vector and Hessian matrix of the image computed in x_o at scale s.

The third term in Equation 2.1 gives the second order directional derivative,

$$\delta x_o^T H_{o,s} \delta x_o = \left(\frac{\partial}{\partial \delta x_o}\right)\left(\frac{\partial}{\partial \delta x_o}\right) L(x_o, s). \tag{2.2}$$

The idea behind eigenvalue analysis of the Hessian is to extract the principal directions in which the local second order structure of the image can be decomposed. Since this directly gives the direction of the smallest curvature (along the vessel) application of several filters in multiple orientations is avoided. This latter approach is computationally more expensive and requires a discretisation of the orientation space.

Let $\lambda_{s,k}$ denote the eigenvalue corresponding to the k-th normalised eigenvector $\hat{u}_{s,k}$ of the Hessian $H_{o,s}$, all computed at scale s. From the definition of eigenvalues:

$$H_{o,s}\hat{u}_{s,k} = \lambda_{s,k}\hat{u}_{s,k} \tag{2.3}$$

it follows that

$$\hat{u}_{s,k}^{T} H_{o,s}\hat{u}_{s,k} = \lambda_{s,k}. \tag{2.4}$$

By analysing Equations (2.2 - 2.4) a nice geometric interpretation arises. The eigenvalue decomposition extracts three orthonormal directions which are invariant up to a scaling factor when mapped by the Hessian matrix. Table 2.1 summarises the relations that must hold between the eigenvalues (λ_k) of the Hessian for the detection of different structures. The eigenvalues are ordered ($|\lambda_1| \leq |\lambda_2|$).

λ_1	λ_2	Orientation pattern
N	N	noisy, no preferred direction
L	H-	tubular structure (bright)
L	H+	tubular structure (dark)
H-	H-	blob-like structure (bright)
H+	H+	blob-like structure (dark)

Table 2.1: Possible patterns in 2D depending on the value of the eigenvalues λ_k (H=high, L=low, N=noisy, usually small, +/- indicate the sign of the eigenvalue). The eigenvalues are ordered: $|\lambda_1| \leq |\lambda_2|$.

For 2D images they propose the following vesselness measure:

$$V_o(s) = \begin{cases} 0 & \text{if } \lambda_2 > 0, \\ exp\left(-\frac{R_B^2}{2\beta^2}\right)\left(1 - exp\left(-\frac{S^2}{2c^2}\right)\right) & otherwise. \end{cases} \tag{2.5}$$

R_B=λ_1/λ_2 is the blobness measure in 2D, β and c are thresholds which control the sensitivity of the line filter to the measures. S is defined as measure of "second order structures",

$$S = \sqrt{\sum_{j \leq D} \lambda_j^2} \tag{2.6}$$

where D is the dimension of the image.

The vesselness measure in Equation 2.5 is analysed at different scales, s. The response of the line filter will be maximum at a scale that approximately matches the size of the vessel to detect. [12] integrate the vesselness measure provided by the filter response at different scales to obtain a final estimate of vesselness.

$$V_o(\gamma) = \max_{s_{min} \leq s \leq s_{max}} V_o(s, \gamma) \tag{2.7}$$

where s_{min} and s_{max} are the maximum and minimum scales at which relevant structures are expected to be found. They can be chosen so that they will cover the range of vessel widths.

2.3 Matched Filter

Matched filtering is another approach to edge detection [10]. The intensity profile varies by a small amount from vessel to vessel and it may be approximated by a Gaussian curve.

$$G(x \mid \mu, \sigma) = \frac{1}{\sigma \sqrt{2\pi}} \exp \frac{-(x-\mu)^2}{2\sigma^2} \tag{2.8}$$

with mean μ and standard deviation σ. Some useful information on two dimensional matched filter can be retrieved in [11].

Consider then the Laplacian of an image $f(x, y)$ smoothed by a Gaussian (expressed using a convolution $*$) . The operation is abbreviated by some authors as LoG, from Laplacian of Gaussian

$$\nabla^2[G(x \mid \mu, \sigma) * f(x, y)]. \tag{2.9}$$

The order of differentiation and convolution can be interchanged because of the linearity of the operators involved

$$[\nabla^2 G(x \mid \mu, \sigma)] * f(x, y). \tag{2.10}$$

The derivative of the Gaussian filter $\nabla^2 G$ can be pre-computed analytically, since it is independent of the image under consideration. Thus, the complexity of the composite operation is reduced.

Finding second derivatives in this way is very robust. Gaussian smoothing effectively suppresses the influence of the pixels that are more than a distance 3σ from the current pixel; then the Laplace operator is an efficient and stable measure of changes in the image. After image convolution with $\nabla^2 G$, the locations in the convolved image where the zero level is crossed correspond to the positions of edges.

This type of filter can be modified and rotated in a template. The rationale is the

correlation between kernel (2D LoG) and signal at different orientations and scales. In fact, it is possible to set up length, width and number of rotation of each filter. Width allows to adjust the filter on vessel calibre and we can track small and tortuous vessels varying the length parameter . The filter gives higher response as its orientation and shape better fit the intensity profile.

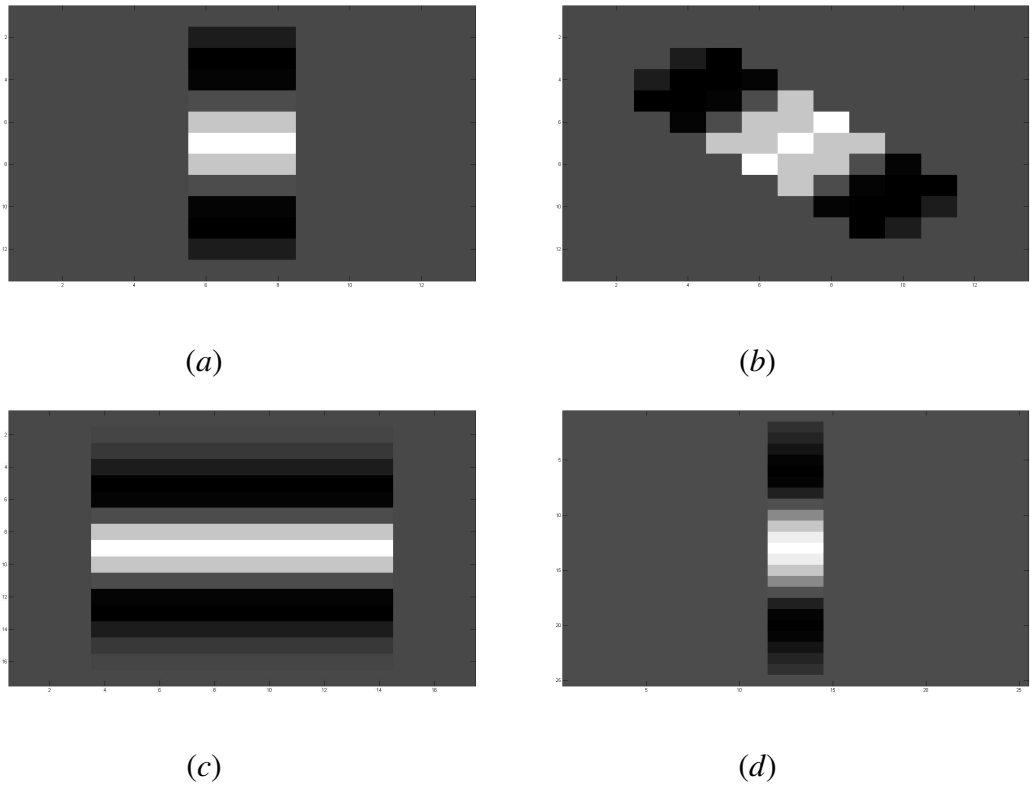

(*a*) (*b*)

(*c*) (*d*)

Figure 2.3: Matched filter template. White is the maximum positive value, black is the maximum negative value. (*a*) Parameters: length=3, width=2 and rotation=0°. (*b*) Length=3, width=2 and rotation=45° (*c*). Length=11, width=2 and rotation=0°. (*d*) Length=3, width=4 and rotation=0°.

In Figure 2.3 we can see some examples of the graphical implementation. These matched filter templates better show the previous considerations. The reference template is in Figure 2.3 (*a*). This template is aligned with zero degrees and has 3 as length and 2 as width. Subfigure (*b*) shows a rotation on 45° of the same filter. If we stretch on the x-axis (left and right directions) we can modify length of the filter template. On the y-axis (up and down direction) width is modified. These last two considerations are shown respectively in Figure 2.3 (*c*) and (*d*).

Chapter 3

Vessel segmentation

This chapter presents a comparison among different methods in vessel segmentation. The presence of noise, the variability of vessel shape and width, the low contrast between vasculature and background make the accurate vessel segmentation a difficult task.

For the comparison, twenty RetCam images, with 130° field of view and 640×480 pixel size, provided by Clarity Medical Systems, CA, USA, were acquired in premature infants with different severity of ROP. A manual segmentation of the vessel network (ground truth) was provided and used to evaluate the performance of the algorithm proposed for vessel extraction.

We use the ground truth without preprocessing to show a realistic analysis. It is possible to use a variance mask on the image for discarding pixels lower than a threshold. However, the correct value of this threshold and the size of the mask are subjective.

In the analysis of red-green-blue (RGB) images, usually the colour components are considered separately because the green channel exhibits the best vessel/background contrast. In few cases also red component might be interesting but very often blue and red ones tend to be very noisy.

3.1 Receiver Operating Characteristic

It is common practise to evaluate the performances of retinal vessel segmentation algorithms using a Receiver Operating Characteristic (ROC) curve. It is a graphical plot which illustrates the performance of a binary classifier system as its discrimination threshold is varied [13].

Starting from the basic concepts, a classification model is a mapping of instances between certain classes or groups. We consider a two-class prediction problem (binary classification) in which the outcomes are labelled either as positive or negative. There are four possible outcomes from a binary classifier. TP is the number of correct

predictions that an instance is positive; FP is the number of incorrect predictions that an instance is negative; FN is the number of incorrect predictions that an instance is positive; TN is the number of correct predictions that an instance is negative. The four outcomes can be formulated in a 2×2 contingency table or confusion matrix, as in Figure 3.1.

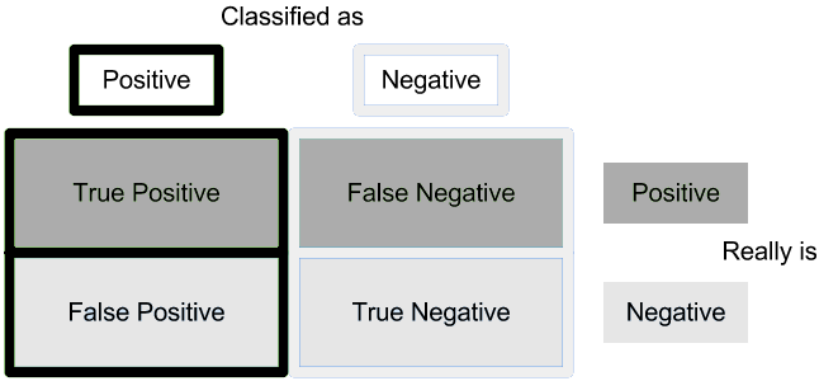

Figure 3.1: Contingency table.

Sensitivity or True Positive Rate	$\frac{TP}{TP+FN}$
Specificity or True Negative Rate	$\frac{TN}{TN+FP}$
Accuracy	$\frac{TP+TN}{TP+TN+FP+FN}$

Table 3.1: Terminology.

ROC curves, constructed from sensitivity and specificity (Table 3.1), do not depend on the decision threshold. In a ROC curve, every possible decision threshold is considered. A ROC curve is a plot of a test's false-positive rate (FPR), or 1-specificity (plotted on the horizontal axis), versus its sensitivity (plotted on the vertical axis). Each point on the curve represents the sensitivity and FPR at a different decision threshold. The plotted (FPR, sensitivity) coordinates are connected with line segments to construct an empiric ROC curve.

A ROC curve begins at the (0, 0) coordinate, corresponding to the strictest decision threshold whereby all test results are negative for disease. The ROC curve ends at the (1, 1) coordinate where all test results are positive for disease.

The line connecting the (0, 0) and (1, 1) coordinates is called the "chance diagonal" and represents the ROC curve of a diagnostic test with no ability to distinguish patients with disease versus those without disease. A test with perfect discrimination

(no overlap in the two distributions) has a ROC curve that passes through the upper left corner. Therefore, the closer the ROC curve is to the upper left corner, the higher the overall accuracy of the test.

3.2 Line Strength

Line strength method is our first local measure of vesselness. In our analysis, we consider the number of rotation as fixed parameter. This value is set at 12, as used in [9]. In this way, we want to underline the importance of different lengths used in the simulations, regardless of the effect of other parameters.

Colour	Length in pixel
Cyan	7
Red	9
Black	11
Blue	13
Green	15
Magenta	17

Table 3.2: Colour legend at different lengths.

Every line is linked to a different colour (Table 3.2) with the aim of showing in a better way each ROC curve. Figure 3.2 shows the mean trend of the twenty images of the dataset.

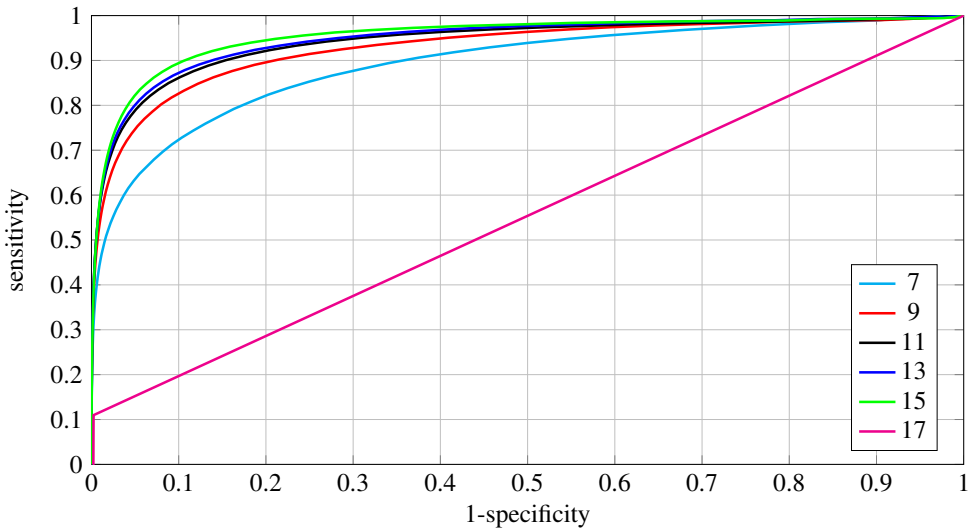

Figure 3.2: ROC curves (mean) for Line Strength.

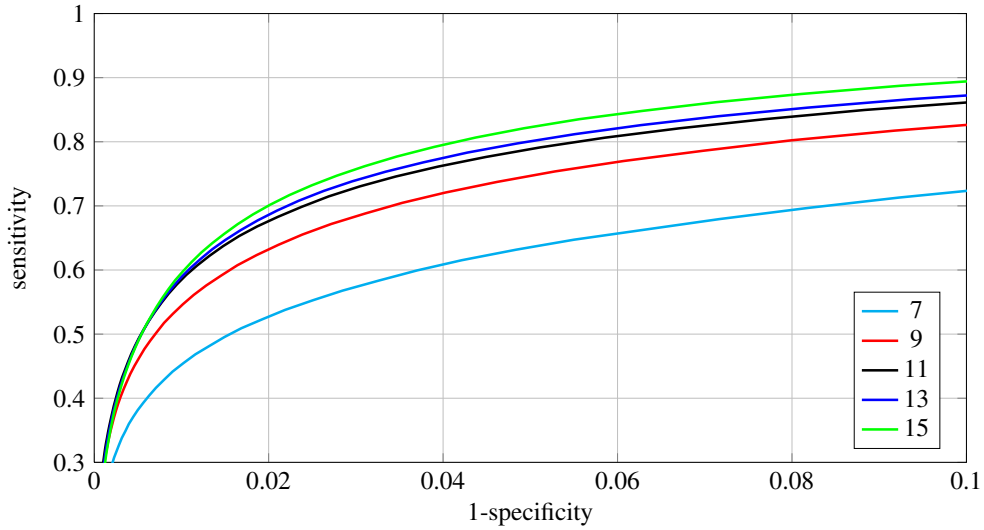

Figure 3.3: A blow-up of ROC curves (mean) for Line Strength.

In Figure 3.3 we can better see different responses at different lengths. In this image there is a blow-up of the previous picture. As before every line is linked to a different colour (Table 3.2).

The curve corresponding to 7 pixels length is the lowest in Figure 3.3. Increasing gradually the length of each line, the ROC curves prove an enhancing of performances in terms of sensitivity and specificity. A high value of specificity means a better capacity to find pixels that are part of vessels. For this reason, we consider almost 0.90 of specificity a satisfactory result in our analysis. On the other hand, sensitivity is linked to the number of false negative and shows the rate of wrong pixels classified as vessels. High sensitivity means few pixels of the background classified as part of vessels.

From Figure 3.3 we observe that the gap between 7 and 9 pixels is very highlighted. There is a difference in terms of space that shows an improvement for the red curve. In fact, the red line is much closer the y-axis and it reaches a higher value of sensitivity than the cyan line on equal values of the x-axis.

From 9 to 11 pixels the difference is lower than the previous two lines. Increasing the number of pixels there is an improvement of the performances and the pick is 15 pixels. Here, the green line shows the best trend. In our analysis this value maximises sensitivity and specificity. This is also the cut off point because at 17 pixels we have worse performances. In fact, the previous trend suggested an enhancement of the performances with an increasing of line length. However, from 17 to more pixels, the algorithm completely fails the vessel detection (see magenta line in Figure 3.2).

3.3 Eigen-decomposition of the Hessian

Eigen-decomposition of the Hessian is linked to the values of the different scales. In Table 3.3 the colour legend at different scales is reported. The ROC curves for the twenty images are shown in Figure 3.4 while in Figure 3.5 we can see a blow-up.

Colour	Scale
Cyan	1
Red	2
Black	3
Blue	4
Green	5

Table 3.3: Colour legend at different scales.

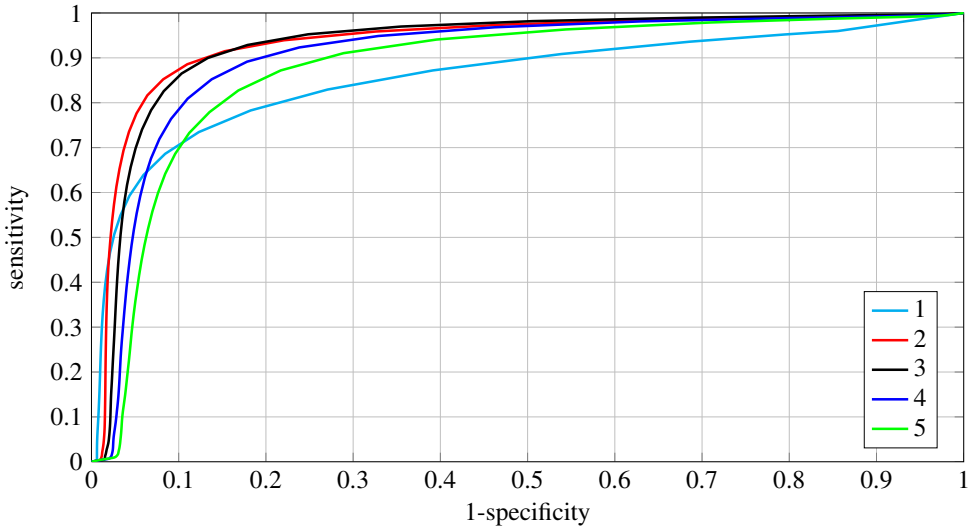

Figure 3.4: ROC curves (mean) for Eigen-decomposition of the Hessian.

Our analysis starts from the lower scale that is drawn in cyan colour. The corresponding ROC curve is very close to the origin and remains parallel to the y-axis until the 0.3 value of sensitivity. In comparison with the other scales, the lowest scale shows the best trend in this part of the graph.

From 0.3 the cyan line becomes curve and in the observation window (Figure 3.5) its maximum value of sensitivity is 0.7, the same of the green line. We can say that scale 1 and scale 5 are the boundaries in terms of performances because the other three scales show an enhancement in terms of accuracy for this dataset. In fact, scale 3 and 4 have similar trend but the first is better than the second one. In Figure 3.5 we can see that the gap between the two ROC curves varies from 0.1 to 0.2 in terms of sensitivity with the black line performing better than the blue line.

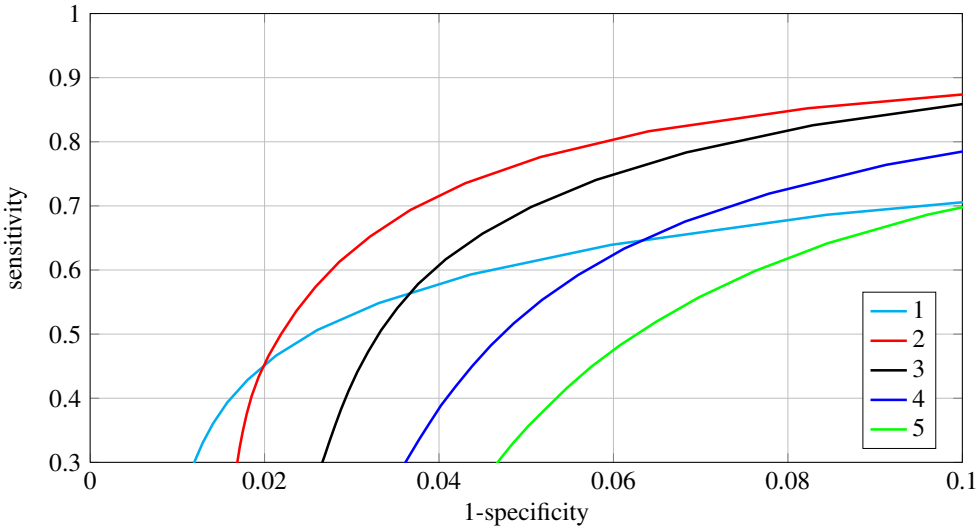

Figure 3.5: A blow-up of ROC curves (mean) for Eigen-decomposition of the Hessian.

Finally, scale 2 is the best. The red line shows the highest value of sensitivity in almost all the trend in the observation window. Table 3.4 summarises the accuracy values. It is reported the mean of the best values of accuracy, computed for each image of the dataset, at different scales.

Scale	Accuracy
1	0.9505
2	0.9517
3	0.9489
4	0.9489
5	0.9488

Table 3.4: Accuracy values at different scales.

3.4 Matched Filter

The discussion about the measure of vesselness for the matched filter is shown using different approach. In fact, this analysis is more complicated than the previous ones.

The most important parameter is width but also length plays a significant role. Table 3.5 reports the accuracy for 5 different width values and for 4 lengths. In total there are 20 values. We use an adaptive threshold that corresponds to the maximum value of accuracy for each filter. The number of rotation is set to an angular resolution of 10°. A total of 36 convolutions are needed.

Width	Length			
	3	**7**	**11**	**15**
1	0.9582	0.9617	0.9626	0.9613
2	0.9650	0.9655	0.9658	0.9649
3	0.9669	0.9672	0.9670	0.9660
4	0.9666	0.9662	0.9658	0.9651
5	0.9652	0.9641	0.9631	0.9626

Table 3.5: Results for the different Matched Filter templates in terms of accuracy.

Figure 3.6 shows the ROC curve for the best value among the accuracy found previously. In this case, the highest value corresponds to 3 as width and 11 as length. However, Table 3.5 proves the possibility of other candidates. The gap among the coloured cells is very small but it should be noted that the width value of 3 gains the three-fourths of the better values. In this case the filter gives higher response as its orientation and shape better fit the intensity profile.

After a limit value, there is a worsening of the performances. In this case, a higher value of length shows the lowest performances in terms of accuracy. On the other hand, only two width values (3 and 4) achieved the expected result.

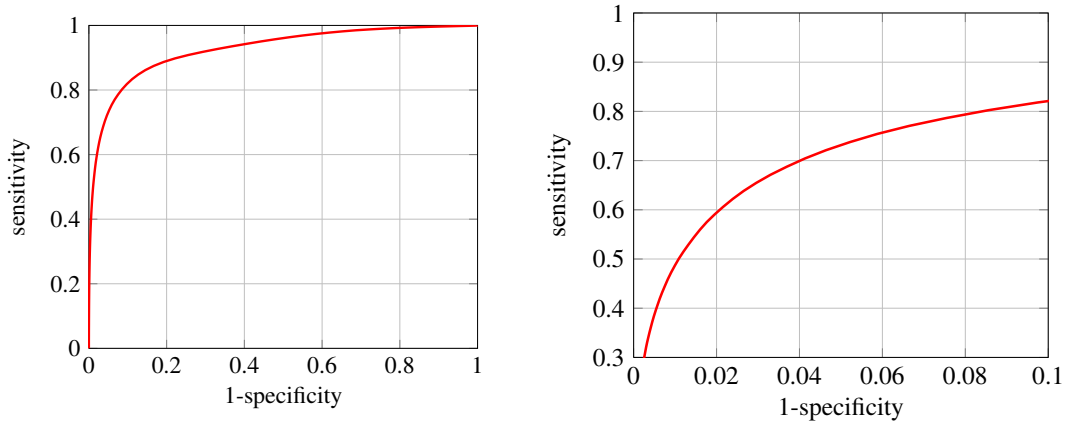

Figure 3.6: ROC curve for the best value of accuracy. Parameters: length=7, width=3.

Figures 3.7-3.14 show a comparison among the best value of accuracy and the surrounding eight cells of Table 3.5. The ROC curve with densely dashed line is the term of comparison while the solid line is the new benchmark. All the figures are not the entire ROC curves but only a blow-up with the most significant parts.

The ROC curves of the eigth cells around the red one show some interesting feautures. In fact, six of eight figures prove the same trend between the two curves. Small

differences are visible but the sensitivity profile remains the same. Only Figures 3.8 and 3.9 disagree with the control line. The first one has a better response at high values of specificity but at 0.1 of the x-axis the two ROC curves are overlapped. On the other hand, Figure 3.9 shows the best trend in the entire observation window. The gap remains costant and it is almost 10% more in terms of sensitivity. Matched filter with length equal to 11 and width equal to 2 provide the best ROC curve trend.

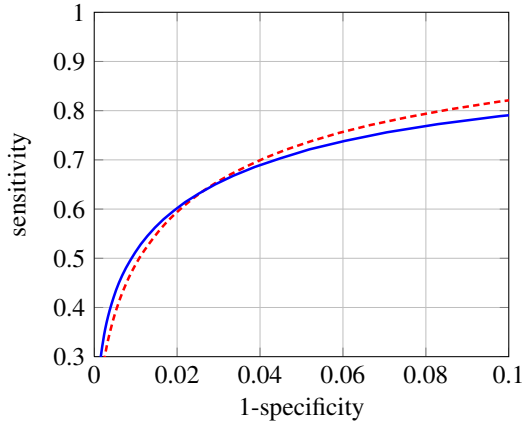

Figure 3.7: Parameters: $l = 3$, $w = 2$ for the solid line; $l = 7$, $w = 3$ for the dotted line.

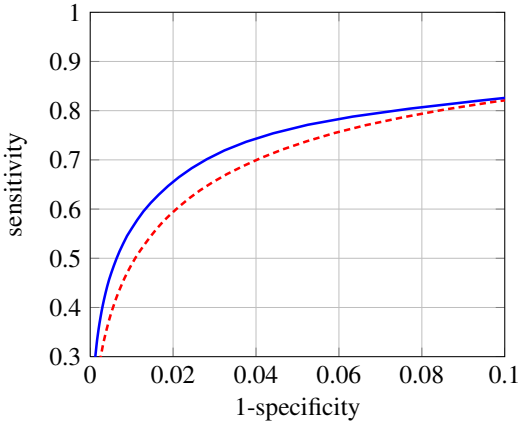

Figure 3.8: Parameters: $l = 7$, $w = 2$ for the solid line; $l = 7$, $w = 3$ for the dotted line.

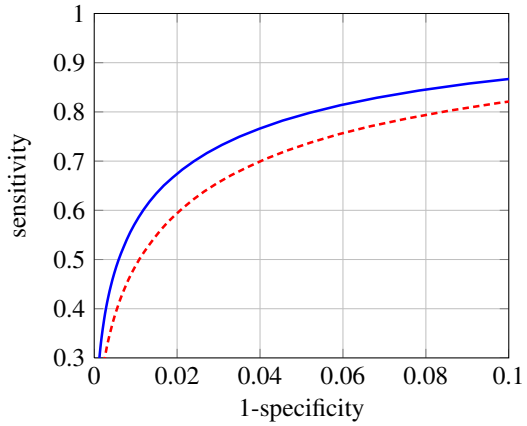

Figure 3.9: Parameters: $l = 11$, $w = 2$ for the solid line; $l = 7$, $w = 3$ for the dotted line.

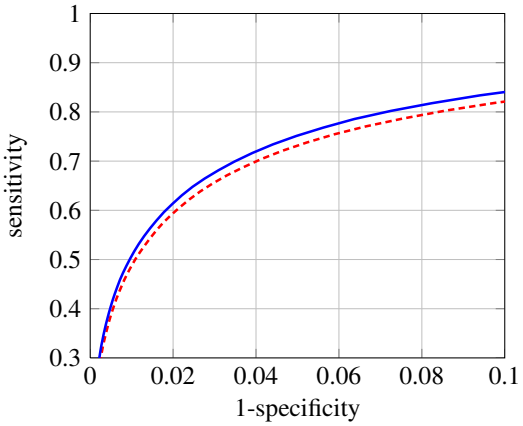

Figure 3.10: Parameters: $l = 3$, $w = 3$ for the solid line; $l = 7$, $w = 3$ for the dotted line.

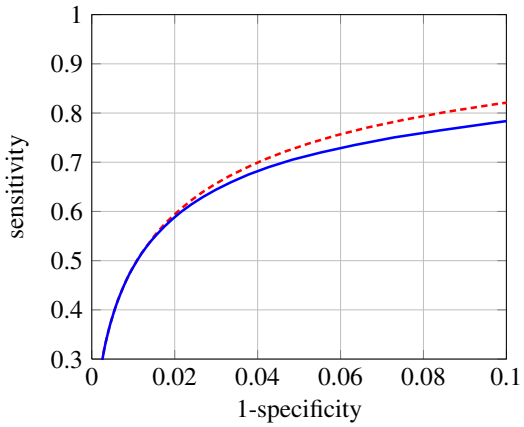

Figure 3.11: Parameters: $l = 11$, $w = 3$ for the solid line; $l = 7$, $w = 3$ for the dotted line.

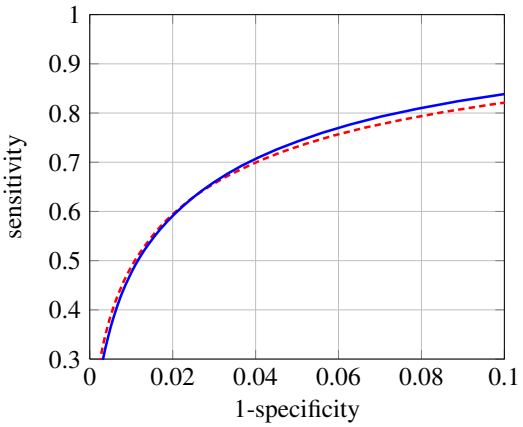

Figure 3.12: Parameters: $l = 3$, $w = 4$ for the solid line; $l = 7$, $w = 3$ for the dotted line.

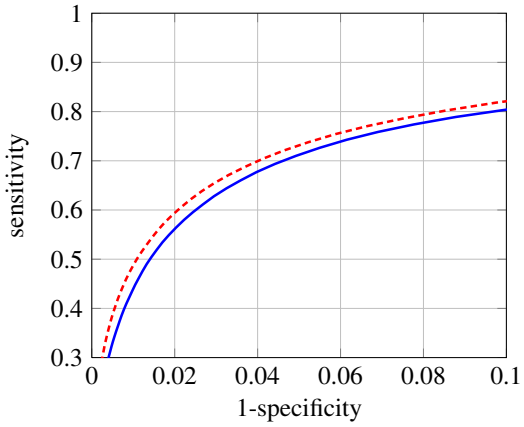

Figure 3.13: Parameters: $l = 7$, $w = 4$ for the solid line; $l = 7$, $w = 3$ for the dotted line.

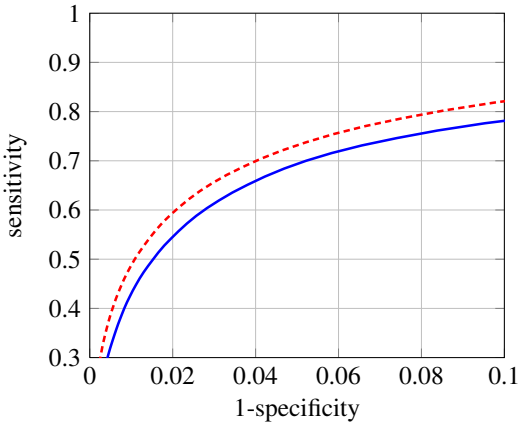

Figure 3.14: Parameters: $l = 11$, $w = 4$ for the solid line; $l = 7$, $w = 3$ for the dotted line.

Chapter 4

Direction coherency measure

In this chapter we compute a new algorithm with the aim of enhancing performances of the previous three methods. This uses a measure of direction to find vessels that have a strong probability to be correctly classified.

From each previous method we obtain the "direction map" that provides an angular value for all the pixels in the image. If a pixel is part of a vessel, it is probably surrounded by pixels that have the same direction. A group of pixels can be interconnected with another group with slightly different angular value and form with it a piece of vessel. Areas where pixels have a random distribution probably belong to the background. On the other hand, the presence of choroidal vessels can be detected as retinal vessels, causing false positive in our analysis. The difference between choroidal and retinal vessels is difficult to find and the algorithm almost always tracks both types.

We report in the following the implementation of our function. It extends the image with zero pixels (zero-padding) like a picture frame. In this way it is possible to use the algorithm for all the pixels. Then, the function selects each pixel and checks its angular value. If in the neighbourhood there are pixels of the same value (or very close) the function "rewards" the chosen pixel. The observing mask can be edited according to the user experience.

In this chapter we use three different masks (3×3, 5×5 and 7×7 pixels). The target value used by the comparison with the ground truth is composed for the 80% of the best vessel measure and the remaining 20% of the output of the new algorithm.

4.1 Line Strength

Figure 4.1 shows the direction coherency measure for the Line Strength method. In this figure the length of the line is 15 pixels, considering 12 angles each of 15 angular resolution, according to the results in Section 3.2.

In Table 4.1 there are the maximum values of accuracy for Line Strength method without postprocessing and using the three different masks.

In Figure 4.1 (*a*) there is the ROC curve for the Line Strength method. In subfigures (*b*), (*c*) and (*d*) there is a comparison among the different sizes of implemented masks using a blow-up of the ROC curves. The densely dashed line is the ROC curve without the direction coherency measure while the solid line is the new benchmark.

None	**Mask**		
	3×3	5×5	7×7
0.9651	0.9649	0.9646	0.9647

Table 4.1: Results in terms of accuracy (length=15).

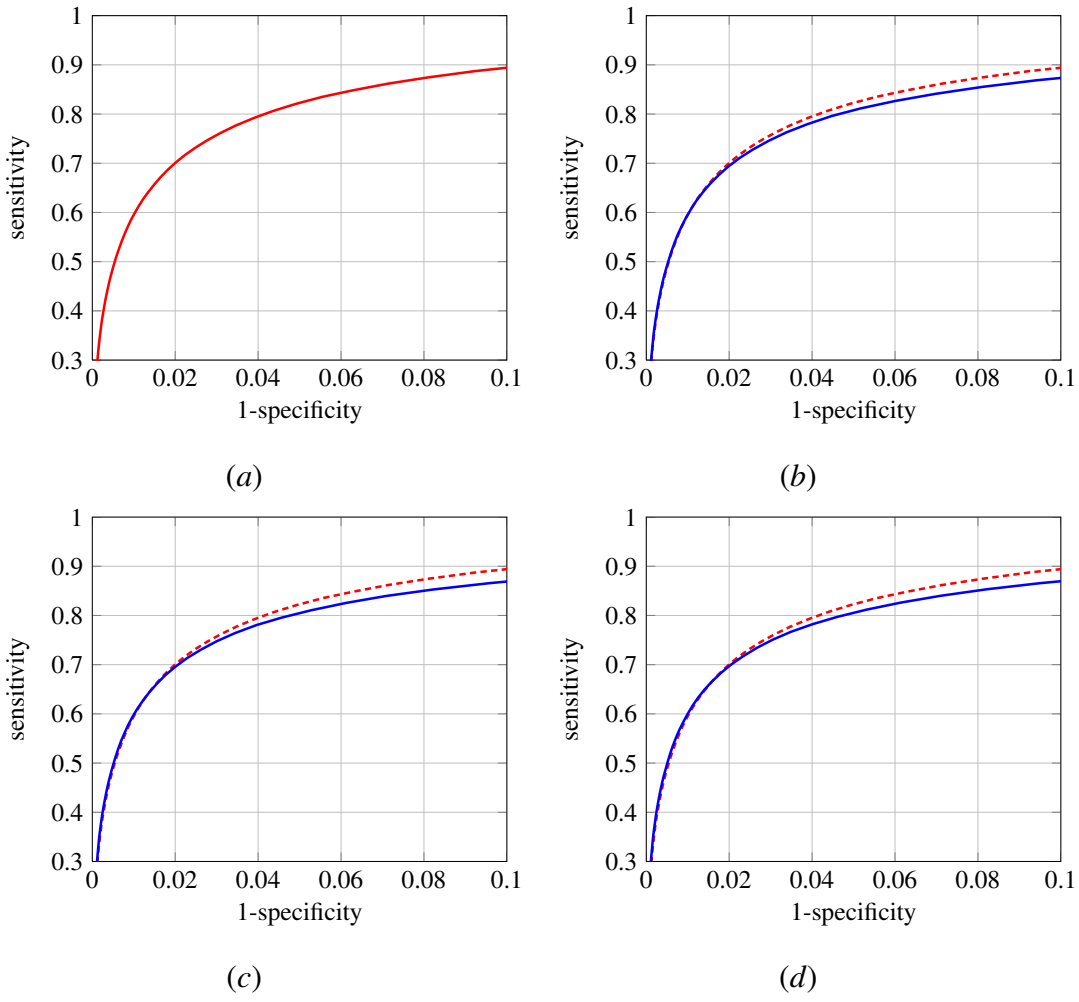

Figure 4.1: ROC curves for Line Strength and after the direction coherency measure. (*a*) Line Strength method (length=15). (*b*) Mask 3×3. (*c*) Mask 5×5. (*d*) Mask 7×7.

After this analysis, we can see that the contribution of the algorithm does not

change the performances of the vesselness measure and it does not increase the accuracy value. Also the best ROC curve holds steady.

4.2 Eigen-decomposition of the Hessian

Table 4.2 shows the maximum values of accuracy for this method and after the direction coherency measure. In Figure 4.2 (*a*) there is the ROC curve for the Eigen-decomposition of the Hessian with scale equal to 2. In subfigures (*b*), (*c*) and (*d*) there is a comparison among the different sizes of implemented masks using a blow-up of the ROC curves. The dashed line is the ROC curve without the direction coherency measure while the solid line is the new benchmark.

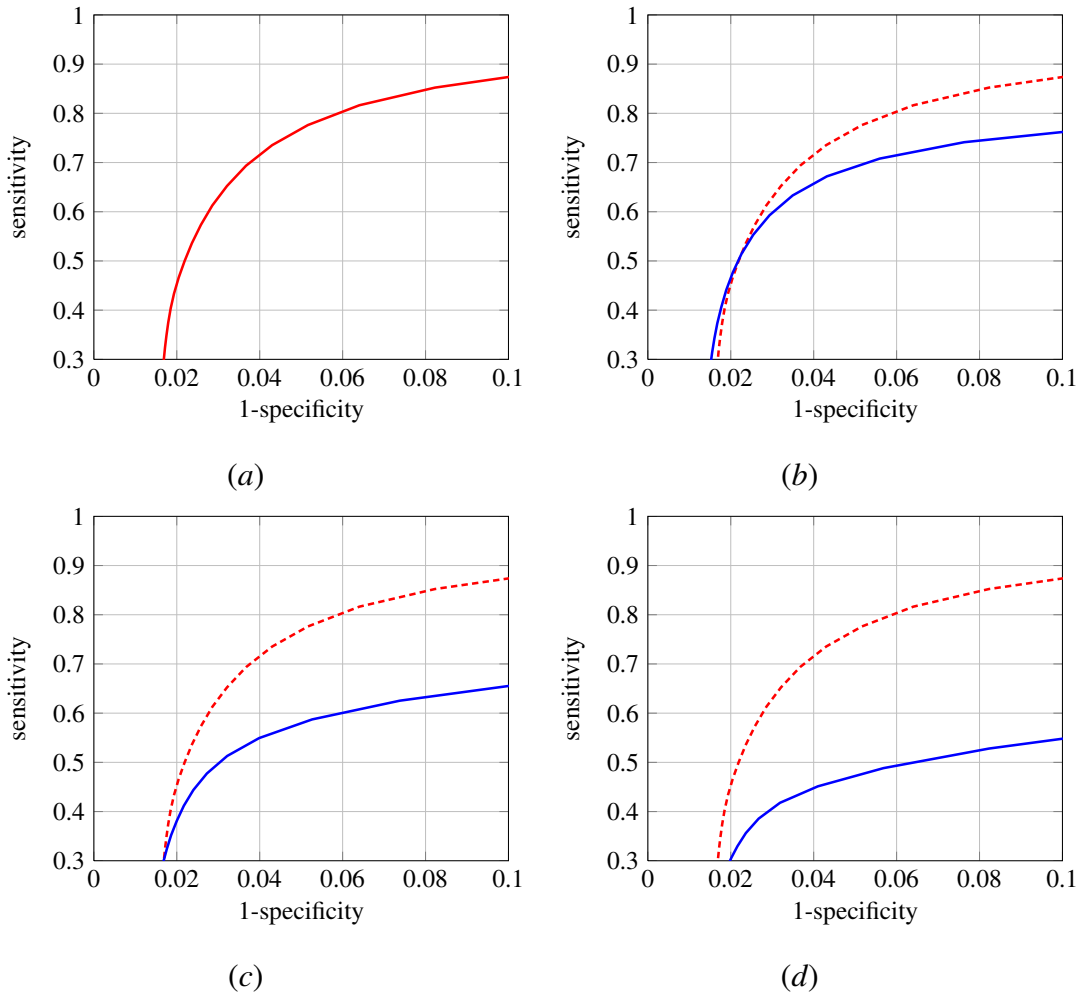

Figure 4.2: ROC curves for Eigen-decomposition of the Hessian and after the direction coherency measure. (*a*) Eigen-decomposition of the Hessian (scale=2). (*b*) Mask 3×3. (*c*) Mask 5×5. (*d*) Mask 7×7.

None		**Mask**	
	3×3	5×5	7×7
0.9517	0.9517	0.9494	0.9489

Table 4.2: Results in terms of accuracy (scale=2).

In this case, there is a loss of quality after the direction measure. In fact, subfigures (*b*), (*c*) and (*d*) show a gap between the ROC curves in spite of the similar value in terms of accuracy. The direction map provided by this method is not acceptable for the subsequent analysis.

4.3 Matched Filter

As the previous sections, in Figure 4.3 (*a*) there is the ROC curve for the matched filter method. In subfigures (*b*), (*c*) and (*d*) there is a comparison among the different sizes of implemented masks using a blow-up of the ROC curves. The dashed line is the ROC curve without the direction coherency measure while the solid line is the new benchmark. Results in subfigure (*a*) are evaluated for the matched filter with length equal to 7 and width equal to 3.

Figure 4.4 has the same structure of Figure 4.3 but different parameters of the matched filter. Length is equal to 11 and width is equal to 2.

Table 4.3 summarises the results with and without the direction method. All the values represent the means of the best accuracies of each image.

None			**Mask**		
	3×3	5×5	7×7	9×9	11×11
0.9672	0.9672	0.9674	0.9675	0.9675	0.9672
0.9658	0.9659	0.9662	0.9664	0.9664	0.9661

Table 4.3: Results in terms of accuracy. In the first line length=7 and width=3. In the second line length=11 and width=2.

The analysis is the same for Figure 4.3 and Figure 4.4. In fact, increasing the mask size, the value of accuracy improves, as outlined in Table 4.3. The cut off value for the size of the mask is 7×7 because after this there are not changes in terms of accuracy and the values hold steady or decrease.

On the one hand, the direction coherency measure increases the accuracy, on the other hand the ROC curves show the same profile. The curves overlap and there is no improvement in the sensitivity profile.

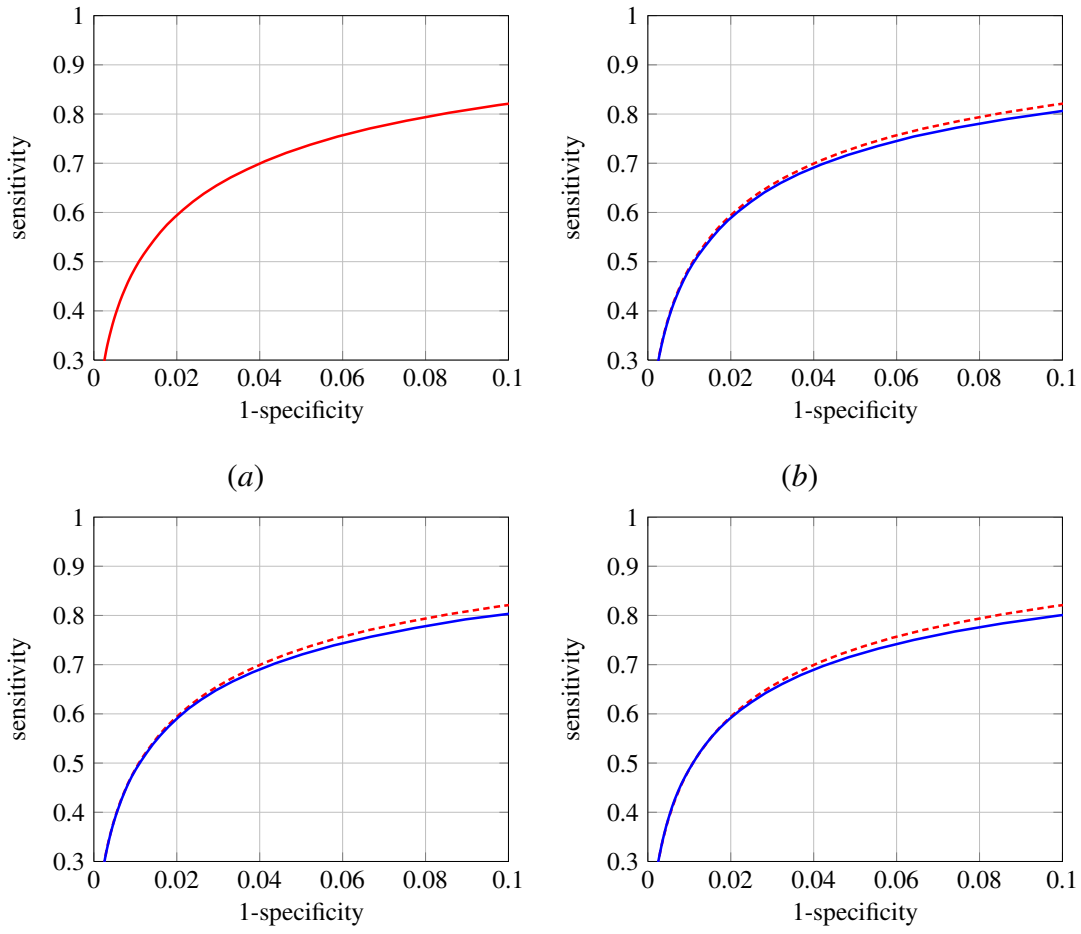

Figure 4.3: ROC curves for Matched Filter and after the direction coherency measure. (*a*) Matched Filter (length=7 and width=3). (*b*) Mask 3×3. (*c*) Mask 5×5. (*d*) Mask 7×7.

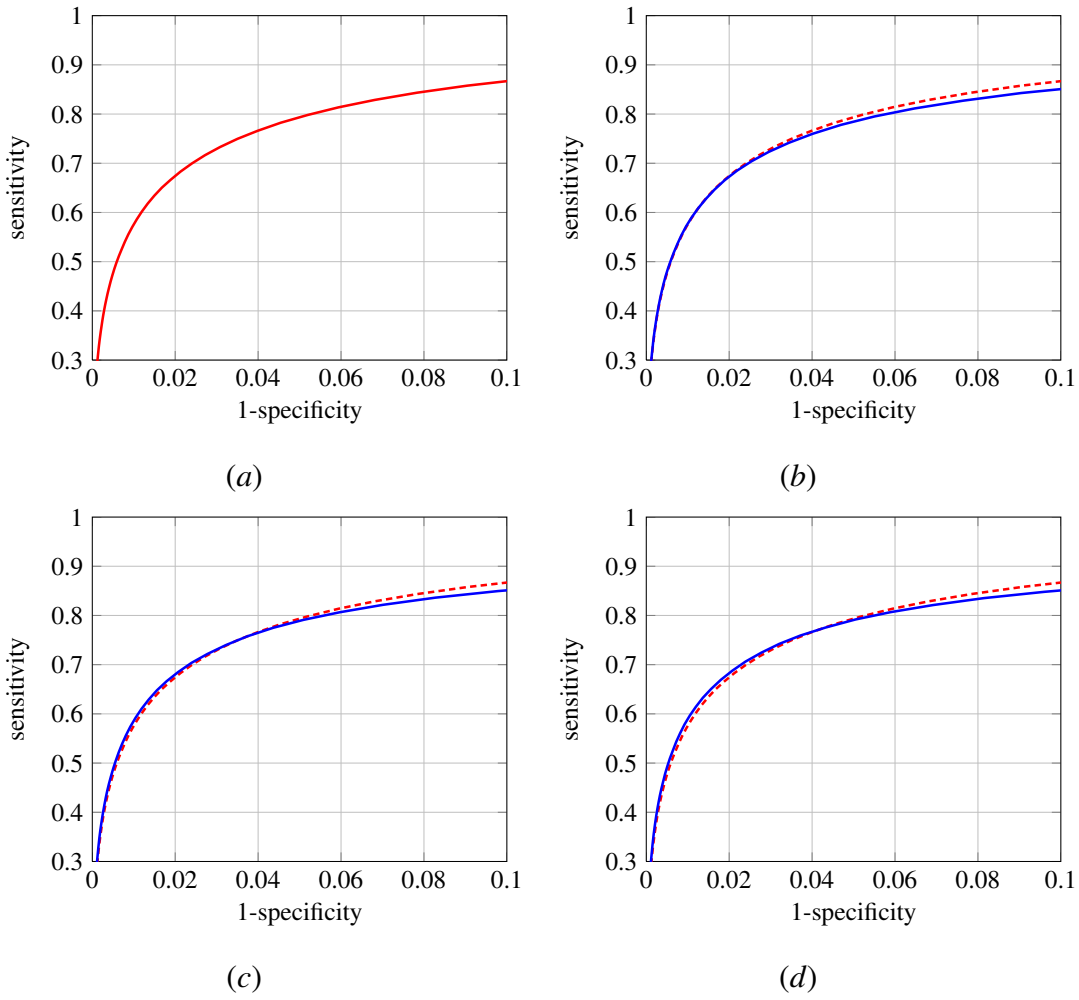

Figure 4.4: ROC curves for Matched Filter and after the direction coherency measure. (*a*) Matched Filter (length=11 and width=2). (*b*) Mask 3×3. (*c*) Mask 5×5. (*d*) Mask 7×7.

Chapter 5

Conclusion

ROP disease is a new field of study for bioimaging groups in all over the world. The aim of this work is to compare the performances of three different vesselness measures. This idea was born from a lack of studies in literature. *Line Strength, Matched Filter* and *Eigen-decomposition of the Hessian* are vesselness measures used for adult images of Diabetic Retinopathy. However the automatic detection of retinal vessels in digital fundus photograph of infants involves several problems as mentioned in Section 1.1.3.

This thesis presents the comparative results in terms of ROC curves and shows the performances of the previous methods. It is difficult to choose a winner because the results can be seen in a subjective way. In fact, the correct trade-off between sensitivity and specificity is difficult to set. Choosing a good criterion to measure the performance of vessel segmentation algorithms is not trivial. Whether one method performs better than another is highly dependent on the application or database in which the algorithm is to be used.

Line strength shows higher ROC curves than the eigen-decomposition of the Hessian in terms of sensitivity. The matched filter proves its adaptability and its capacity to track all types of vessels. The filter gives higher response as its orientation and shape better fit the intensity profile. In this case, using more lengths and widths at the same time, the resulting vesselness analysis could be more accurate. However, the scope of this study is to present a linear analysis without increasing the complexity of the problem.

The direction coherency measure gives different results depending on the used method. Only the matched filter shows a good trend while the other two methods worsen the performances. The reasons for this are linked to the quality of direction maps that in turn depend on the quality of the images. In the near future, an improving of quality of RetCam images can help automatic detection of vessel analysis.

Bibliography

[1] DK. Wallace, Z. Zhao, SF. Freedman, *A pilot study using ROPtool to quantify plus disease in retinopathy of prematurity*, J AAPOS, Vol. 11(4), pp. 381-387, 2007.

[2] C. Swanson et al, *Semiautomated computer analysis of vessel growth in preterm infants without and with ROP*, Br J Ophatlmol, Vol. 87(12), pp. 1474-1477, 2003.

[3] R. Gelman et al, *Diagnosis of plus disease in retinopathy of prematurity using Retinal Image multi Scale Analysis*, Invest Ophthalmol Vis Sci, Vol. 46(12), pp. 4734-4738, 2005.

[4] E. Poletti et al, *Automatic vessel segmentation in wide-field retina images of infants with Retinopathy of Prematurity*, in Proc. IEEE EMBC 2011, pp. 3954-3957, 2011.

[5] Committee for the Classification of Retinopathy of Prematurity, *The International Classification of Retinopathy of Prematurity revisited*, Arch Ophthalmol, 2005.

[6] T. L. Terry, *Retrolental fibroplasia in the premature infant: V. Further studies on fibroplastic overgrowth of the persistent tunica vasculosa lentis*, Trans Am Ophthalmol Soc 42:383-396.

[7] AM Roth, *Retinal vascular development in premature infants*, Am J Ophthalmol 84:636-640, 1977.

[8] I. I. K. Ahmed and L. D. MacKeen, *A New Approach to Imaging the Angle*, Glaucoma Today, pp. 27-30, July 2007.

[9] E. Ricci, R. Perfetti, *Retinal Blood Vessel Segmentation Using Line Operators and Support Vector Classification*, Medical Imaging, IEEE Transactions on, 2007.

[10] M. Sonka, V. Hlavac, R.Boyle, *Image Processing, Analysis and Machine Vision - 3rd Ed*, Thomson Engineering, 850 p., 2007.

[11] S. Chaudhuri et al, *Detection of Blood Vessels in Retinal Images using Two-Dimensional Matched Filters*, IEEE Transactions on Medical Imaging, 1989.

[12] A. Frangi et al, *Multiscale vessel enhancement filtering*, In Proc. 1st MICCAL, 1998.

[13] C. Metz, *ROC Methodology in Radiologic Imaging*, Investigative Radiology, vol 21, no. 9, pp 720-733,1986.

[14] R. Zwiggelaar, S.M. Astley, C. R. M. Boggis, and C. J. Taylor, *Linear structures in mammographic images: Detection and classification*, IEEE Trans. Med. Imag., vol. 23, no. 9, pp. 1077-1086, Sep. 2004.

List of Figures

1.1 Cross sectional view of the human eye. 2
1.2 Two examples of wide-field ROP image. 4

2.1 Twelve orientations to evaluate line strength of shaded pixel. 8
2.2 (a) Basic line detector. (b) Line detector with its orthogonal line. . . . 8
2.3 Matched filter template. White is the maximum positive value, black is the maximum negative value. (*a*) Parameters: length=3, width=2 and rotation=0°. (*b*) Length=3, width=2 and rotation=45° (*c*). Length=11, width=2 and rotation=0°. (*d*) Length=3, width=4 and rotation=0°. . . 11

3.1 Contingency table. 14
3.2 ROC curves (mean) for Line Strength. 15
3.3 A blow-up of ROC curves (mean) for Line Strength. 16
3.4 ROC curves (mean) for Eigen-decomposition of the Hessian. 17
3.5 A blow-up of ROC curves (mean) for Eigen-decomposition of the Hessian. 18
3.6 ROC curve for the best value of accuracy. Parameters: length=7, width=3. 19
3.7 Parameters: $l = 3$, $w = 2$ for the solid line; $l = 7$, $w = 3$ for the dotted line. 20
3.8 Parameters: $l = 7$, $w = 2$ for the solid line; $l = 7$, $w = 3$ for the dotted line. 20
3.9 Parameters: $l = 11$, $w = 2$ for the solid line; $l = 7$, $w = 3$ for the dotted line. 20
3.10 Parameters: $l = 3$, $w = 3$ for the solid line; $l = 7$, $w = 3$ for the dotted line. 20
3.11 Parameters: $l = 11$, $w = 3$ for the solid line; $l = 7$, $w = 3$ for the dotted line. 21
3.12 Parameters: $l = 3$, $w = 4$ for the solid line; $l = 7$, $w = 3$ for the dotted line. 21

3.13 Parameters: $l = 7$, $w = 4$ for the solid line; $l = 7$, $w = 3$ for the dotted line. 21
3.14 Parameters: $l = 11$, $w = 4$ for the solid line; $l = 7$, $w = 3$ for the dotted line. 21

4.1 ROC curves for Line Strength and after the direction coherency measure. (*a*) Line Strength method (length=15). (*b*) Mask 3×3. (*c*) Mask 5×5. (*d*) Mask 7×7. 24
4.2 ROC curves for Eigen-decomposition of the Hessian and after the direction coherency measure. (*a*) Eigen-decomposition of the Hessian (scale=2). (*b*) Mask 3×3. (*c*) Mask 5×5. (*d*) Mask 7×7. 26
4.3 ROC curves for Matched Filter and after the direction coherency measure. (*a*) Matched Filter (length=7 and width=3). (*b*) Mask 3×3. (*c*) Mask 5×5. (*d*) Mask 7×7. 28
4.4 ROC curves for Matched Filter and after the direction coherency measure. (*a*) Matched Filter (length=11 and width=2). (*b*) Mask 3×3. (*c*) Mask 5×5. (*d*) Mask 7×7. 29

List of Tables

2.1 Possible patterns in 2D depending on the value of the eigenvalues λ_k (H=high, L=low, N=noisy, usually small, +/- indicate the sign of the eigenvalue). The eigenvalues are ordered: $|\lambda_1| \leq |\lambda_2|$. 9

3.1 Terminology. 14
3.2 Colour legend at different lengths. 15
3.3 Colour legend at different scales. 17
3.4 Accuracy values at different scales. 18
3.5 Results for the different Matched Filter templates in terms of accuracy. 19

4.1 Results in terms of accuracy (length=15). 24
4.2 Results in terms of accuracy (scale=2). 27
4.3 Results in terms of accuracy. In the first line length=7 and width=3. In the second line length=11 and width=2. 27

Ringraziamenti

Cominciamo con i ringraziamenti formali. In primis, ringrazio il professor Alfredo Ruggeri per la possibilità datami nello sviluppare una tesi interessante e innovativa. Ringrazio l'ing. Enea Poletti per il lavoro svolto insieme, condito da tanta pazienza per le mie sviste. Un grazie anche per le chiacchierate informali che hanno arricchito questi mesi di lavoro. Ringrazio la mia famiglia e la nonna per la sempre puntuale attenzione nei miei confronti, per il sostegno economico e morale in tutti questi anni di studio. Ringrazio zio Bruno e famiglia per avermi sempre fatto sentire importante e per essersi spesso interessati alla mia carriera universitaria.

Ora vorrei cimentarmi in ringraziamenti particolari. L'ispirazione viene dal telefilm Scrubs, in particolare dall'ultima puntata dell' ottava stagione. J.D. si trova nel corridoio dell'ospedale e immagina che due ali di folla lo salutino al termine del suo periodo al Sacro Cuore. A salutarlo e incoraggiarlo sono tutti i personaggi apparsi nella serie, dalle persone speciali fino ai semplici camei.

Ecco, la fine dell'università per me significa questo. Vedo la fine del mio percorso di studi ma non posso fare a meno di girarmi indietro e ringraziare tutte le persone che ho conosciuto in questi anni padovani. Non farò nomi per non scontentare nessuno ma penso che chi mi ha conosciuto si veda riflesso nei personaggi che andrò a citare.

I primi sono i compagni del collegio, gli ingegneri e i medici che hanno diviso con me gran parte delle giornate. Per chi l'elettronica è una ragione di vita e ha diviso per tanti anni la stanza con un futuro chirurgo amante del teatro; chi ha passato le notti a guardare telefilm e chi gli è stato sempre insieme; chi è venuto a rubare bibanesi e caramelle Big Fruit in camera mia ma che ha sempre messo una parola simpatica dopo ogni furto; chi ha bussato tutti i giorni alla mia porta quando ritornava da lezione ma che poi ha cambiato città; chi nella musica ha trovato la sua grande passione. L'università non è stata facile ma da subito ho incontrato ottimi colleghi. C'è chi passa le ferie a girare il mondo e chi invece vincerà la paura e prenderà presto l'aereo; chi ha passato con me giornate intere in biblioteca ma ha sempre mantenuto il sorriso anche dopo un'intensa giornata di lavoro; chi ha spesso cercato di ammazzarmi ma che in fondo mi vuole molto bene; chi si è concesso uno spritz oppure una pizza serale per rinsaldare un'amicizia. Le pause caffè sono sempre state dei momenti magici. In par-

ticolare, una di queste pause è stata la scintilla che mi ha fatto rincontrare una ragazza speciale. Dopo 5 anni, di caffè ne ho presi tanti ma con lei sono rimasti sempre unici. La mia vita padovana a questo punto si è aperta a nuove conoscenze e la bicicletta mi ha portato in Via Coronelli. Conoscere un'intera famiglia non è mai facile ma anche questo fu amore a prima vista. Tra gli amici di Padova vorrei ringraziare chi una casa la sta costruendo per coronare un amore profondo e chi invece ha scelto di vivere in Germania per inseguire una brillante carriera. L'Erasmus è stata una parentesi incredibile che mi ha fatto incontrare persone favolose e apprezzare le bellezze locali. Il gruppo italiano come sempre si è distinto per l'ironia, la spigliatezza e la tanta voglia di divertirsi. C'è chi sfoggiato capelli colorati e chi mi ha quasi convinto a fabbricare una bomba atomica; chi aveva una propria religione da seguire e certe scelte gli erano imposte, anche se la carta igienica rimane ancora un mistero; chi ha invaso la cucina con mille teglie e che all'occorrenza trovava in me il suo fido assistente.

Grazie a tutti per questi anni passati insieme. Da domani si comincia una nuova avventura, con persone nuove e forse lontano da Padova, ma so che voi rimarrete sempre un pezzo unico della mia vita.